SSIM 2021 - PM Dight (ed.)

doi:10.36487/ACG_repo/2135_04

Case study: open pit three-dimensional slope stability back-analysis for an anisotropic iron ore rock mass

L Figueiredo *Anglo American, Brazil*

M Barros *Anglo American, Brazil*

R Hammah *Rocscience Inc., Ghana*

Y Santos *Walm Engenharia Ltda., Brazil*

T Souza *Walm Engenharia Ltda., Brazil*

C Nogueira *Walm Engenharia Ltda., Brazil*

Abstract

The challenges of representing geotechnical failure mechanisms in software is being gradually addressed as search algorithms and computing power advance, especially to deal with complex anisotropic rock masses in which failure mechanisms are commonly three-dimensional (3D). This paper presents a case study of an iron ore mine with highly anisotropic rock mass strength that has been back-analysed using 3D limit equilibrium analysis methods. In order to provide as realistic model inputs as possible, field characterisation data and the reconstruction of the failed surface were used, as well as the material properties available from laboratory tests or bibliographic references. A probabilistic approach was applied to the initial parameters, resulting in a series of stochastic simulations that provided scenarios for the failure moment, when the Factor of Safety achieved close to 1.0. Then, based on the knowledge of the local geological-geotechnical context and failure mechanisms, a range of values for the geomechanical parameters were achieved to enhance the constitutive model of the rock mass.

Keywords: *three-dimensional limit equilibrium, open pit slope stability, anisotropic iron rock masses, back-analysis*

1 Introduction

Evaluating mine slope stability requires a deep knowledge of the excavated rock mass in order to identify failure mechanisms, given the uncertainties inherent to the geotechnical properties.

The open pit case study is located at Serra do Sapo, Brazil, the deposit is commonly mined as benched footwall slopes following the dip of the itabirite ore, resulting in relatively shallow overall slope angles (around 28°).

Regionally, the deposit trends in a north-northwest–south-southeast direction, and is stratigraphically inversed and characterised by a system of thrust faults. Foliation is generally subparallel to faults and dips around 30° to the east. Figure 1 shows a typical section where it is possible to observe the stratigraphic inversion and the main lithologic domains at Serra do Sapo.

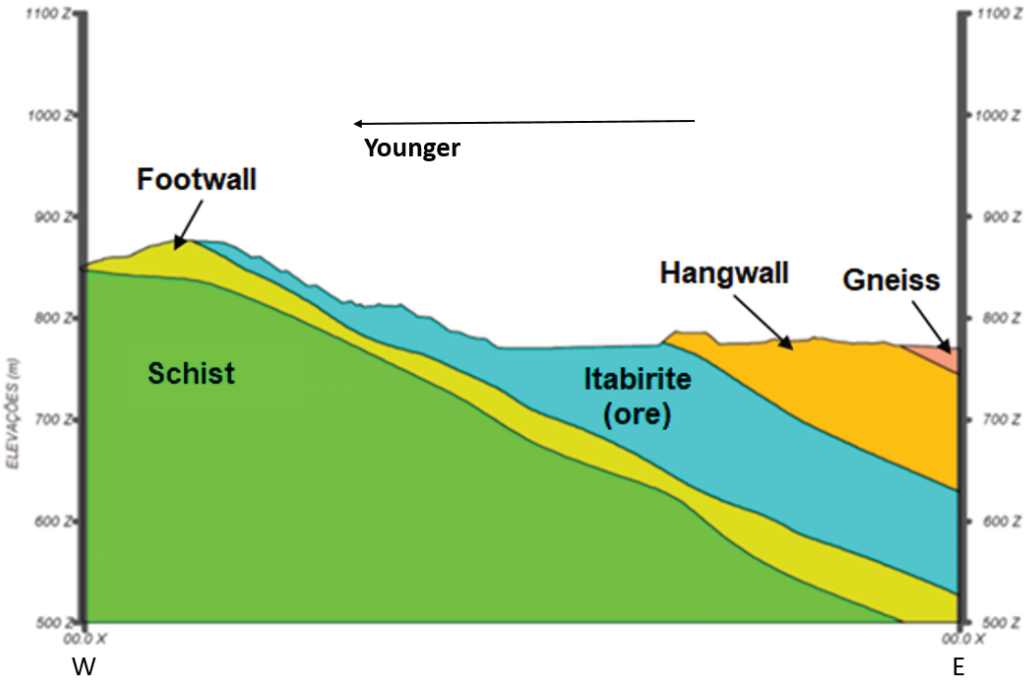

Figure 1 Serra do Sapo's typical section, showing the stratigraphic inversion and the main lithologic domains

The failure mechanism in Serra do Sapo's open pit is controlled by the strong anisotropy imposed by faults parallel to the foliation and to the geological contacts. This anisotropy has influence on the three different scales of potential failure mechanisms, bench, inter-ramp and overall slope failure, depending on the persistence, character of the various discontinuities and the slope geometry.

And the most critical failure mechanism is the footwall contact between the ore (itabirite) and the waste rock (quartzite), in which shear zones and lenses of phyllite intercalated with quartzite occur. This material is named 'phyllonite' and can occur in this shear zones and also in lenses internal to the itabirite as shown in Figure 2.

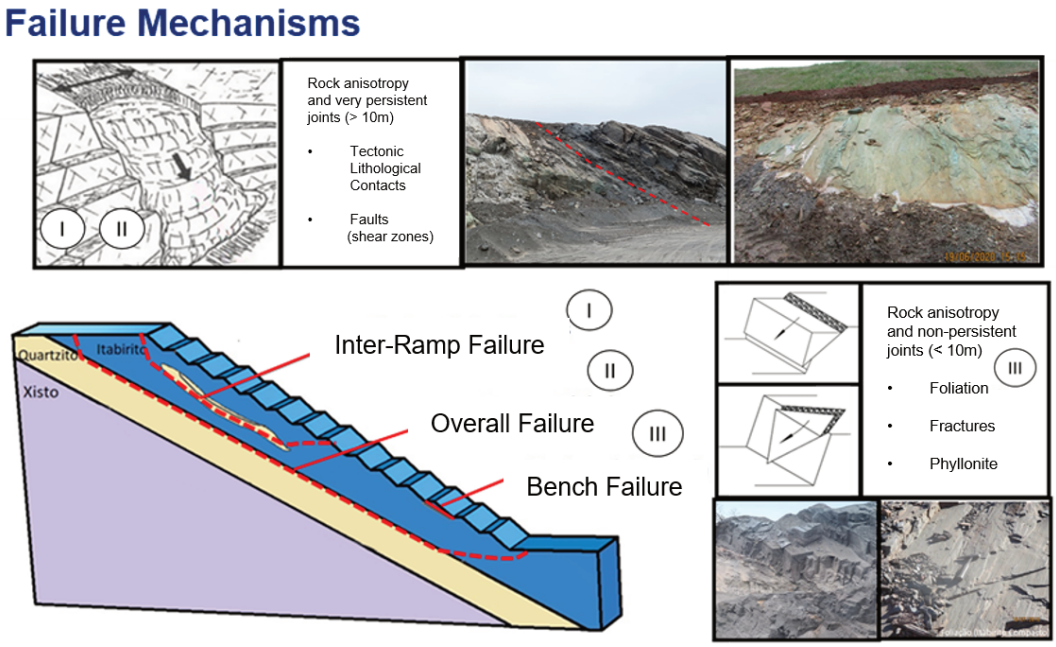

Figure 2 Main controlling factors of the failures in the slopes of Serra do Sapo's open pit

2 Failure history

In 2018, a slope failure occurred in Serra do Sapo's open pit during the rainy season, compromising six benches below the pit's main access ramp. Figure 3 indicates the area where the failure event took place.

Figure 3 Failure event in 2018

The first evidence of instability was identified in 2016 from displacements observed in prisms due to the deepening of the mining at the site (Figure 4). There were no impacts in terms of safety, as the monitoring strategy and trigger action response plan (TARP) worked properly, establishing exclusion zones, above and below the failure, timely to avoid some event. However, in terms of material losses, the blocked area below restricted the mining and, at the above area, closed the half main ramp of the mine in that time, impacting production as well.

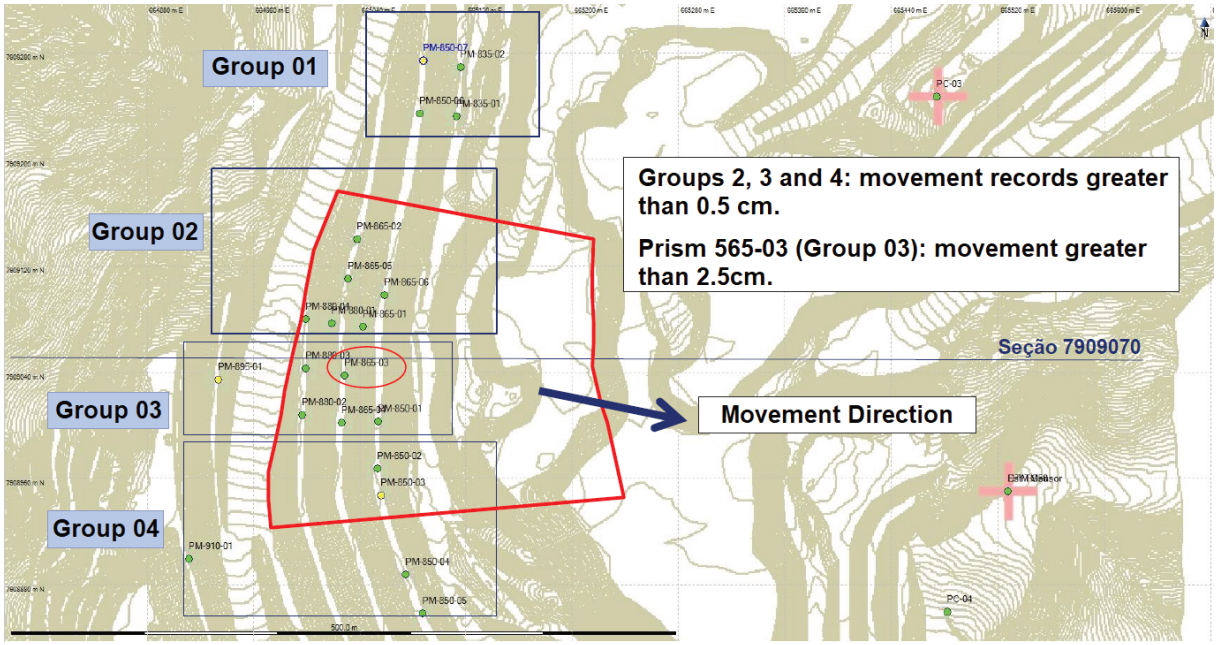

Figure 4 Prisms monitoring in 2016

Based on the TARP, monitoring intensification took place with the installation of radar in order to achieve a real-time monitoring of displacements. Due to these actions, it was possible to identify the major event in 2018 in advance. Figure 5 presents the failure surface identified by radar monitoring.

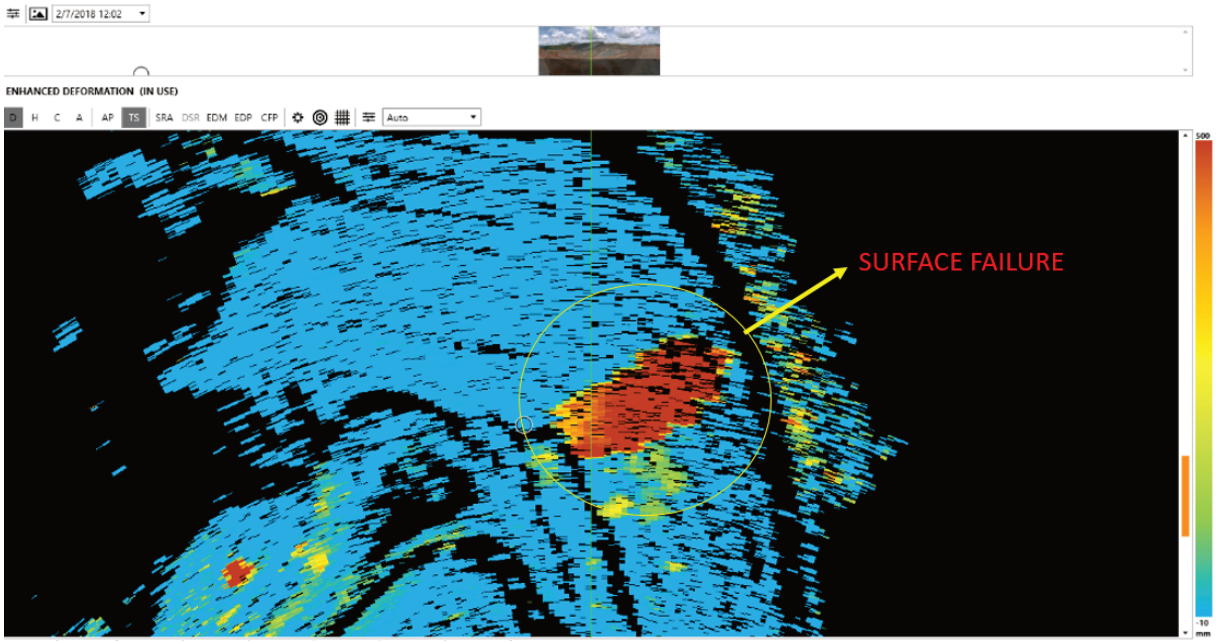

Figure 5 Failure surface identified in the radar in 2018

3 Methodology

The methodology was based on the reconstruction of the failed surface in 3D, combined with back-analysis of the failure. The back-analysis started with the parameterisation of the rock mass and definition of the initial parameters for the failure surface, gathered from field observations and bibliography.

In order to understand the correlation coefficient and statistical relationship between the parameters and the Factor of Safety, probabilistic analysis was completed as well as sensitivity analysis of the water level.

4 Model setup

4.1 Modelling strength functions

Initially, the failure mechanism and the strength criteria that better represent the constitutive model for the material involved in the event were verified. From mapping and borehole data, it was possible to identify that the 'phyllonite' conditioned the failure event due to its low strength parameters and low permeability coefficient. In general, phyllonite occurs in the contact between the itabirite and the footwall's quartzite, being this material (phyllonite) characterised by low thickness phyllite lenses with high persistence and low strength throughout the quartzite in the shear zone, as shown in Figure 6. Thus, it was decided to model this material as a surface/discontinuity once this approach better represents the failure. It was verified that one of the factors that lead to the failure event was the low thickness of the itabirite in the slope face, leaving the exposure of the phyllonite contact too close to the slope face.

Figure 6 Examples of phyllonite in the field with low thickness phyllite lenses with high persistence and low strength throughout the quartzite in the shear zone

With regards to the strength criteria for the phyllonite, the Barton & Bandis (1983) criterion was used in the back-analysis, since the phyllonite behave as a singular structure of low thickness in the shear contact. The Barton–Bandis criterion is non-linear and widely used to model the shear strength of rock discontinuities. The Barton & Choubey (1977) equation for the shear strength in relation to the normal stress is given by Equation 1:

$$\tau = \sigma_n \tan\left[\phi_r + JRC \log_{10}\left(\frac{JCS}{\sigma_n}\right)\right] \quad (1)$$

where:

ϕ_r = residual friction angle.

JRC = joint roughness coefficient.

JCS = joint wall compressive strength.

The value of the basic friction angle (ϕ_b) was estimated, as proposed by Barton & Choubey (1977) and others, based on the minerals present in the surface. Table 1 presents the basic friction angle values for the minerals as a reference. As the phyllonite surface is mostly composed by muscovite, the value for ϕ_b of 23° was considered. It is worth mentioning that for the current study, the residual friction angle is considered to be equal or very close to the basic friction angle due to the composition of the phyllonite.

Table 1 Values of friction angle (ϕ_b) between mineral surfaces. Extracted from Mitchell & Soga (2005)

Mineral	Type of test	Conditions	ϕ_b	Comments	Reference
Muscovite	Along cleavage faces	Dry	23.3	Oven dry	Horn & Deere (1962)
		Dry	16.7	Air equilibrated	
		Saturated	13.0		

4.2 Rock bridge estimates

Rock bridges that could affect the failure surface strength were also considered, being the calculations regarding the friction angle based in the formulations proposed by Dershowitz et al. (2017) and Jennings (1972). From these references, the percentage of the rock bridge is given by the coefficient of continuity along the failure pathway (k) as shown in Equations 2 and 3.

$$Rock\ Bridge\ Percentage = 1 - k \tag{2}$$

$$k = \frac{\sum l_j}{\sum l_j + \sum l_r} \tag{3}$$

where:

- l_j = length of joints.
- l_r = length of rock bridges.
- k = coefficient of continuity along the failure pathway.

Thus, *k* = 10 m / 12 m ≅ 0,83.

Rock bridge percentage = 1 - *k*

Rock bridge percentage = 1 - 0,80 = 20%

The values of 10 m for the joint length (l_j) and 2 m for the length of rock bridges (l_r) were estimates based on field mapping of the joint persistence. The rock bridges are not visible unless the rock mass is exposed.

From the estimate of the *k* coefficient, it is possible to calculate the equivalent friction angle of the failure surface according to Equation 4, as proposed by Jennings (1972) as shown below.

$$\tan\left(\phi_{eq}\right) = (1-k)\tan(\phi) + k.\tan\left(\phi_j\right) \tag{4}$$

where:

- ϕ_{eq} = friction angle of the equivalent discontinuity.
- ϕ = friction angle of the rock bridges.
- ϕ_j = friction angle of the joints within the rock mass.
- *k* = coefficient of continuity along the failure pathway.

Thus, the equivalent friction angle of failure surface in the phyllonite can be calculated:

$$\tan\left(\phi_{eq}\right) = (1-0.80).\tan(25) + 0.80.\tan(20)$$

$$\tan\left(\phi_{eq}\right) = 0.415$$

$$\phi_{eq} \cong 23°$$

The friction angle value of the rock bridge (25°) is related to the quartzite parameters, which were taken from the averages of the CIUsat triaxial tests. Figure 7 schematically presents the phyllonite layer and the estimated rock bridges in relation to the analysed slope.

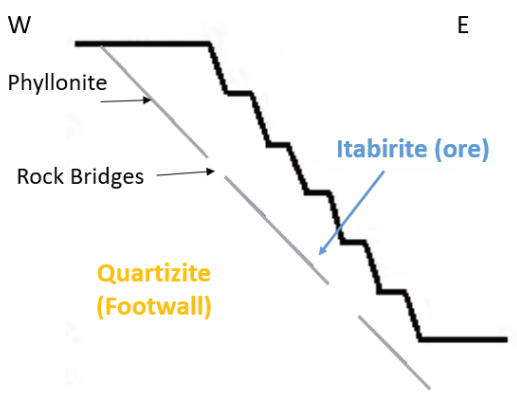

Figure 7 Phyllonite layer and the estimated rock bridges in relation to the analysed slope

4.3 Shear strength properties

The values of joint compressive strength (JCS) were estimated by strength evaluation by the International Society for Rock Mechanics (ISRM) standard methods for the field classification of rock strength, leading to the classification of the surface as 'very weak rock' as shown in Table 2 where the JCS ranges are exhibited.

Table 2 List of joint compressive strength. Extracted from RocData from Rocscience Inc®

Material	Description	Joint compressive strength range (MPa)
Soil	Very soft clay	<0.025
Soil	Soft clay	0.025–0.05
Soil	Firm clay	0.05–0.10
Soil	Stiff clay	0.10–0.25
Soil	Very stiff clay	0.25–0.50
Soil	Hard clay	>0.50
Rock	Extremely weak rock	0.25–1.0
Rock	Very weak rock	1.0–5.0
Rock	Weak rock	5.0–25
Rock	Medium strong rock	25–50
Rock	Strong rock	50–100
Rock	Very strong rock	100–250
Rock	Extremely strong rock	>250

The values of joint roughness coefficient (JRC) were defined by the characterisation of the failure surface roughness, measured in field surveys. Table 3 presents the roughness characterisation.

Table 3 Roughness characterisation of the failure surface

Structure	Description	Jr	JRC 200 mm	JRC1 m
Failure surface	Planar - smooth	1.0	1.5	0.9
(Phyllonite)	Planar - rough	1.5	2.5	2.3

It is observed that the JCS and JRC parameters vary with the scale factor, as these parameters are greatly reduced with the increase in scale (Barton & Bandis 1990), as presented in Figure 8.

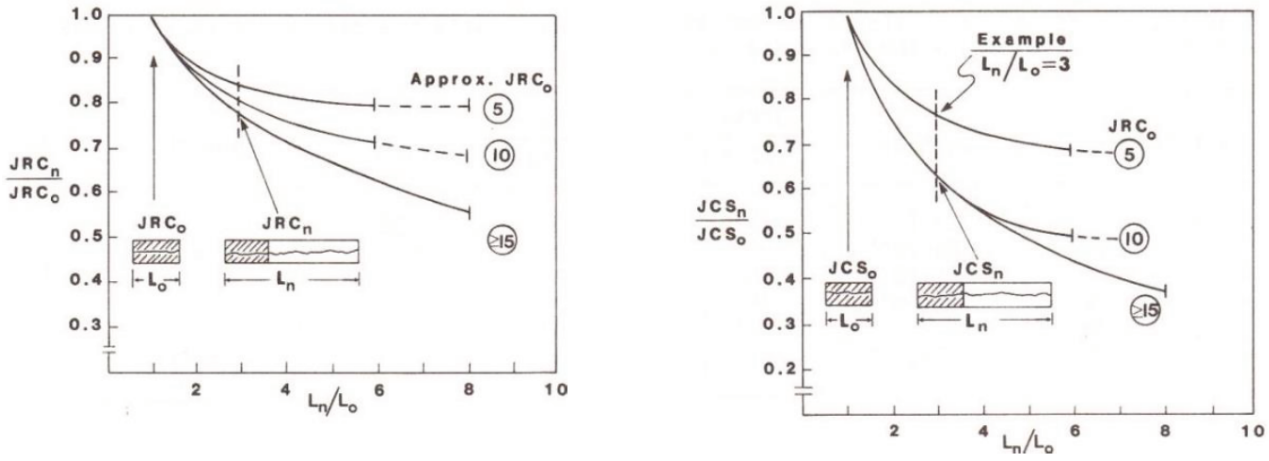

Figure 8 Joint roughness coefficient (JRC) and joint compressive strength (JCS) parameters relation by the scale factor. Extracted from Barton & Bandis (1990)

Table 4 presents the Barton & Bandis (1990) parameters initially adopted for the phyllonite surface in the stability analyses. These parameters were defined according to the data presented in the previous items, and it is worth mentioning that these are initial values that will be varied in the back-analysis.

Table 4 Barton & Bandis (1990) strength parameters initially adopted for the phyllonite surface

Material	ID	Barton & Bandis			
		γ (KN/m^3)	Joint roughness coefficient	Joint compressive strength (kPa)	ϕ_{eq}* (°)
Phyllonite	FIL	20	2	2000	23

*Calculated value scaled to account for the effects of rock bridging.

5 Modelling methodology

5.1 Strength functions

Finally, a probabilistic approach was used in the back-analysis for the solution of the problem. The phyllonite strength parameters were considered as random variables whose average parameters, variability, and distribution type adopted are shown in Table 5.

The coefficients of variation adopted were 5% for the specific weight, 45% for the JRC, 30% for the JCS, and 13% for the basic friction angle. These adopted coefficients were based on typical values according to Assis (2020) and it is important to observe that engineering evaluation was applied to the range of possible values in a way to not allow negative values for these variables.

Table 5 Barton & Bandis (1990) strength parameters initially adopted for the phyllonite surface

Variable	Mean value	Standard deviation	Statistical evaluation (3 × standard deviation)	Probability distribution
Specific weight (KN/m^3)	20	1	17 (23)	Normal
Joint roughness coefficient	2	0.9	1 (3)	Triangular
Joint compressive strength (kPa)	2000	600	200 (3,800)	Normal
ϕb (°)	23	3	14 32	Normal

Besides the phyllonite surface parameters, the stability analyses also considered the parameters from the other materials involved in the problem, which are itabirite, footwall quartzite, and the schist also located in the footwall. For these materials, the Mohr–Coulomb criteria was adopted and the parameters were estimated by consolidated undrained triaxial and direct shear laboratory tests, data from prior back-analysis and also by the experience with the behaviour of these materials.

Table 6 shows the adopted parameters for the materials involved in the back-analysis. The shear strength parallel or perpendicular are associated with the rock anisotropy.

Table 6 Mohr–Coulomb shear strength parameters for the lithotypes involved in the back-analysis

Material	ID	Specific weight		Perpendicular strength		Parallel strength	
		ɣnat (KN/m3)	ɣsat (KN/m3)	c' (kPa)	ϕ' (°)	c' (kPa)	ϕ' (°)
Friable itabirite	IF	22	24	50	36	25	29
Friable quartzite	QTF	20	22	50	28	30	25
Friable schist	XIF	17	19	13	36	13	33

It was necessary to reconstruct the failure surface by an estimation based on the available data, such as the topography before and after the event, field data, geologic contacts, and radar displacement information. Figure 9 shows a reverse view of the failure surface modelled in 3D in relation to the slope in Serra do Sapo's open pit. It is important to highlight that this surface coincides with the phyllonite contact defined in the previous item of this paper as the conditioning material of the failure event.

Figure 9 Reverse view of the estimated failure surface

5.2 Analysis and search method

After the determination of the contributing factors of the failure event and the estimative of the strength parameters for the involved materials, back-analysis was conducted using a probabilistic approach. For this, variations were applied to the initial parameters as presented, resulting in a series of stochastic simulations that provided scenarios for the failure moment, when the safety factor reached 1.0 or close.

3D limit equilibrium stability analysis was conducted using the software Slide 3 (Rocscience Inc. 2021). The following criteria and assumptions were adopted in this analysis:

- Surface type: Ellipsoid.
- Search method: Cuckoo.
- Optimisation: surface altering with 20 iterations.
- Method of analysis was used: Morgenstern-Price and Bishop.
- For the anisotropic materials presented in Table 6, the 'anisotropic strength' strength criteria (present in the software Slide3) was used, with values of A and B of 3 and 8, respectively.
- For the phyllonite, the Barton & Bandis (1990) strength criteria was used and the failure surface was modelled as a weak layer with the phyllonite parameters.
- For the water level criteria, the phyllonite surface was considered as saturated, using the water surface methodology.

Figure 10 shows the results of the deterministic and probabilistic stability analysis performed by the entrance parameters described. Figure 11 presents the frequency histograms of the parameters involved in the probabilistic analyses.

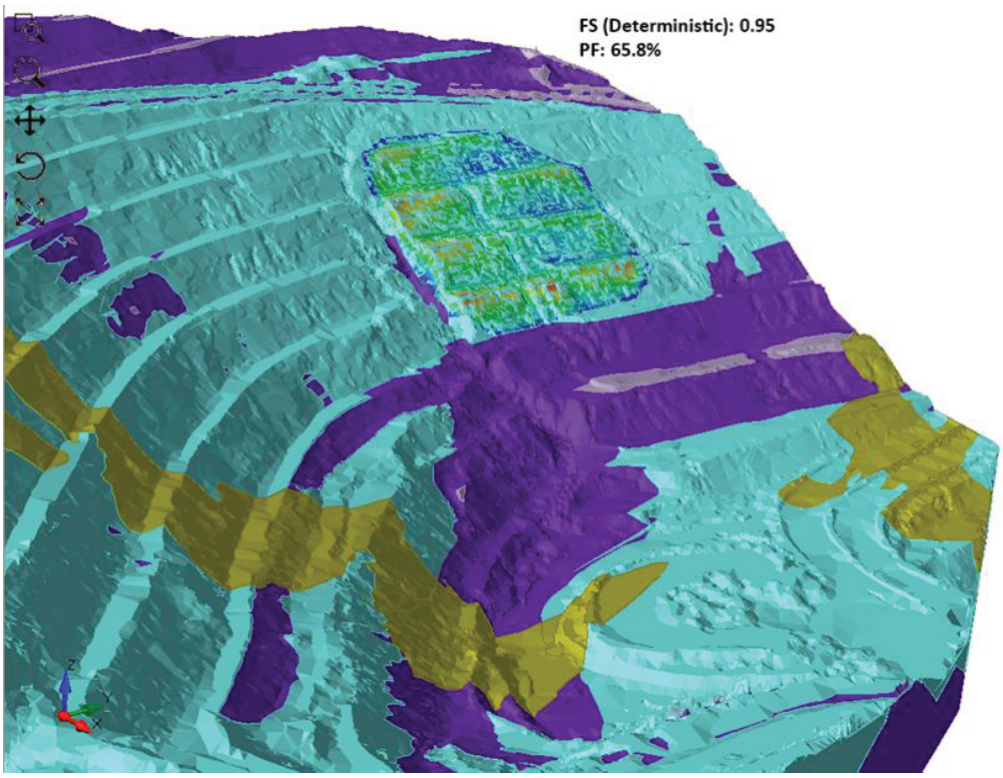

Figure 10 Deterministic and probabilistic result obtained by the stability analysis performed in the software Slide3

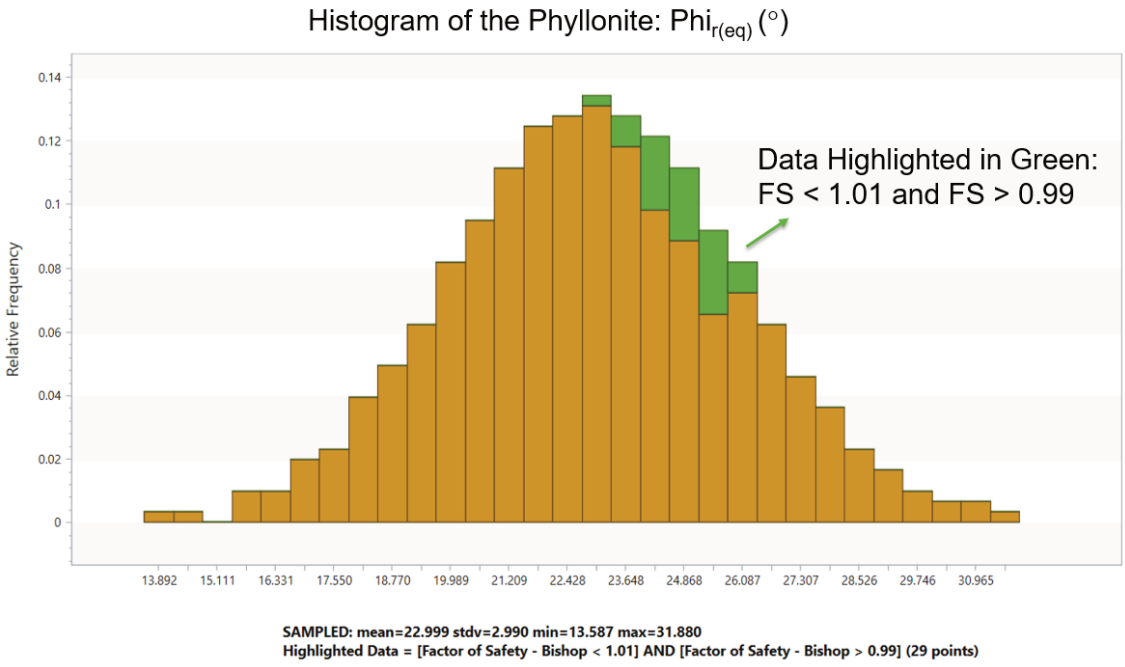

Figure 11 Frequency histogram of the Phyllonite phi$_{r(eq)}$ involved in the sensitivity analyses

From the evaluation of the parameters variation histograms, it is possible to verify that the friction angle is the most relevant parameter to the variation of the safety factor. This can be supported by the correlation graphics presented in Figure 12, where not only the correlation between the variation of the parameters and the safety factor is shown, but also the parameter value evaluated when the safety factor is 1, i.e. when the slope is in imminence of instability.

Figure 12 Correlation graphics for the parameters involved in the back-analysis and relation with the safety factor

Another parameter that was posteriorly variated was the water level, once it exerts great influence in the stability analysis and consequently provokes changes in the parameters obtained by back-analysis. No hydrogeological monitoring instruments were available for the date of the failure. Thus, it was necessary to estimate a transient water level that could be generated by water infiltrating from rain, percolating in the itabirite that has a higher permeability coefficient, and that may not have percolated so easily in the phyllonite, leading to elevated pore pressures along the contact. Figure 13 presents the simulated water levels positions in the sensitivity analyses.

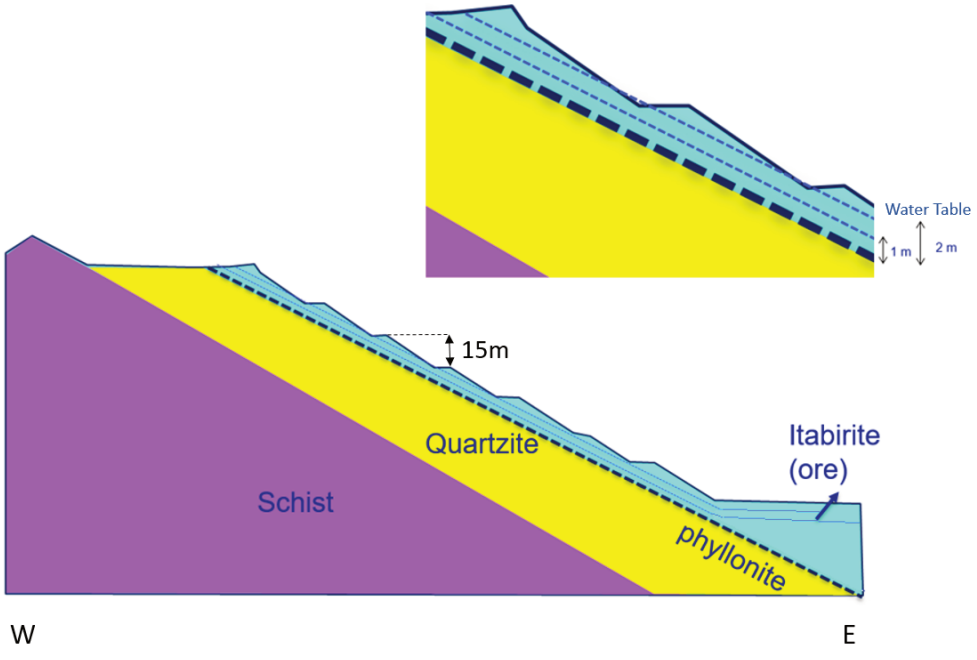

Figure 13 Simulated water levels: sensibility analyses

Thus, Table 7 shows the results obtained in the back-analyses performed from the premises presented and developed in this paper.

Table 7 Back-analyses results

Factor of Safety (FS = 1.0)			
Watertable (m)*	**ϕr (°)**	**Joint compressive strength (MPa)**	**Joint roughness coefficient**
0 (dry)	23	2	1.5
1	24	2	2
2	30	2	2.5

*Perpendicular distance of the watertable above the phyllonite surface.

By comparing the results of the back-analysis with the parameters initially estimated, it is possible to recognise that the initial parameters were well estimated and are very close to those obtained in the back-analysis. This is probably due to the field observations and characterisations.

6 Conclusion

The analyses performed became possible due to the enhancement of the knowledge over the geomechanical behaviour of the contact zone between the ore and the footwall. Back-analyses is a good way to evaluate and get the structure parameters that are difficult to sample and test in a laboratory.

Thus, from this study, it was possible to increase the reliability of the parameters and of the pit stability analyses. The use of sophisticated computational analysis, such as 3D limit equilibrium with new tools to refine the surface search and probabilistic approach, could simulate with accuracy the failure mechanism. It is verified that the surface with the lower safety factor obtained by deterministic stability analysis approaches the failure that took place in 2018, as presented in Figure 14. The difference in the lateral limits of the surfaces, as shown in Figure 14, must have occurred due to erosive or structural components that limited the surface.

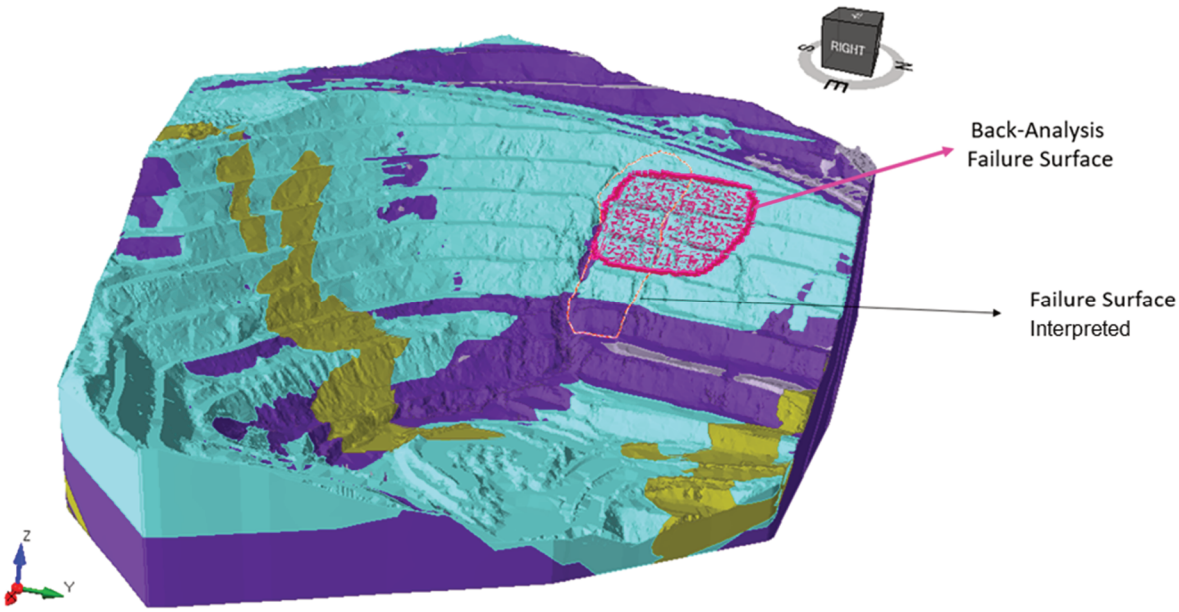

Figure 14 Comparison between the surface obtained in the back-analysis and that interpreted by radar information

The parameters obtained by back-analyses are coherent to the expected based on observational and bibliographic data over the phyllonite material but we still need additional sample collection and laboratory testing to build a larger database on shear strength of the phyllonite. It's worth mentioning that a test campaign is currently being carried out with the sampling of this material.

From the analyses, it was shown that a greater command of the friction angle in this case study and the low correlation coefficient of the JCS may be a reflection of the lack of confinement at the toe of the slope. For future studies, it is necessary to verify the thickness of intact rock that is required to separate the phyllonite from the slope face to achieve an adequate Factor of Safety (1.2–1.3).

Another recommendation is the installation of hydrogeological instruments to investigate the real-time influence of pore pressure on this contact, mainly in the rainy season.

References

Assis, AP 2020, 'Risk management for geotechnical structures: consolidating theory into practice', *Soils and Rocks*, vol. 43, no. 3, pp. 311–336.

Barton, NR & Bandis, S 1983, 'Effects of block size on the shear behaviour of jointed rock issues in rock mechanics', *Proceedings of the 23rd US Symposium on Rock Mechanics*, Society of Mining Engineers of AIMS, Berkeley, pp. 739–760.

Barton, NR & Bandis, S 1990, 'Review of predictive capabilities of JRC-JCS model in engineering practice', in N Barton & O Stephansson (eds), Proceedings of the International Symposium of Rock Joints, AA Balkema, Rotterdam, pp. 603–610.

Barton, N & Choubey, V 1977, 'The shear strength of rock joints in theory and practice', *Rock Mechanics*, pp. 10, no. 1, pp. 1–54.

Dershowitz, WS, Finnila, A, Rogers, S, Hamdi, P & Moffitt, KM 2017, 'Step path rock bridge percentage for analysis of slope stability', *Proceedings of the 51st US Rock Mechanics/Geomechanics Symposium*, American Rock Mechanics Association, Alexandria.

Horn, HM & Deere, DU 1962, 'Frictional characteristics of minerals', *Géotechnique,* vol. 12, no. 4, pp. 319–335.

Jennings, JE 1972, 'An approach to the stability of rock slopes based on the theory of limiting equilibrium with a material exhibiting anisotropic shear strength', *Proceedings of Stability of Rock Slopes*, American Society of Civil Engineers, New York, pp. 269–302.

Mitchell, JK & Soga, K 2005, *Fundamentals of Soil Behavior*, vol. 3, John Wiley & Sons, New York.

Rocscience Inc. 2021, *Slide 3*, computer software, Rocscience Inc., Vancouver.